Near-Field Hybrid Beamforming Design for mmWave Integrated Sensing and Communication

Minghao Yuan*, Dongxuan He*, Hao Yin†, Yuyang Liu*, Ziqi Kang*, and Hua Wang*
*School of Information and Electronics, Beijing Institute of Technology, Beijing 100081, China
†Institute of China Electronic System Engineering, Beijing 100141, China
Email: minghaoyuan@bit.edu.cn, dongxuan_he@bit.edu.cn, yinhao@cashq.ac.cn,
3220195096@bit.edu.cn, ziqi_kang@bit.edu.cn, wanghua@bit.edu.cn

2025 IEEE 102nd Vehicular Technology Conference (VTC2025-Fall) | 979-8-3315-0320-8/25/$31.00 ©2025 IEEE | DOI: 10.1109/VTC2025-Fall65116.2025.11310280

***Abstract*—In this paper, we investigate near-field hybrid beamforming design for millimeter-wave (mmWave) integrated sensing and communication (ISAC) systems, where one base station (BS) equipped with large-scale antenna array simultaneously serves multiple communication users and performs target localization by exploiting the degrees of freedom in both angle and distance domains. First, to characterize the target localization accuracy, we analyze the squared position error bound (SPEB) for estimating the two-dimensional (2D) position of target. Then, the hybrid beamforming design is formulated to maximize the sum-rate of communication users, while guaranteeing the SPEB constraint of target localization, transmit power constraint, and constant modulus constraints. To tackle the nonconvex problem, we propose a fractional programming (FP) and successive convex approximation (SCA)-based block coordinate descent (BCD) algorithm. Simulation results demonstrate that the proposed hybrid beamforming can achieve sum-rate close to fully-digital beamforming and outperform the baseline schemes.**

***Index Terms*—Integrated sensing and communication, near-field, target localization, squared position error bound, hybrid beamforming.**

I. Introduction

Integrated sensing and communication (ISAC) has been widely recognized as a key technology for empowering various emerging applications, such as intelligent transportation and low-altitude economy [1]. To meet the demand for high-capacity communication and high-accuracy sensing, sixth-generation (6G) wireless communication systems are evolving towards extremely large-scale antenna arrays and high frequencies [2]. The increased array aperture and carrier frequency result in the paradigm shift of electromagnetic characteristics, i.e., from the planar-wave-based far-field propagation to the spherical-wave-based near-field propagation [3]. Compared to the far-field channel, the near-field channel introduces an extra degree of freedom in the distance domain. Leveraging both distance and angle information incorporated in the spherical-wave model, near-field communication can concentrate beam energy on specific positions, thereby achieving high-resolution beamfocusing [4]. Moreover, the spherical wavefront can be exploited to achieve target localization through joint distance and angle estimation [2]. Therefore, near-field ISAC technologies have received considerable interest [5].

Beamforming is a critical technique to realize high-speed data transmission and high-accuracy target sensing simultaneously. Recently, the potential of near-field ISAC beamforming has been widely explored [6]–[8]. Specifically, in [6], beamforming design for multiuser near-field ISAC systems was investigated to minimize the Cramér-Rao bound (CRB) for joint distance and angle sensing while satisfying the communication rate requirement of each user. The authors in [7] proposed a near-field beamforming scheme to improve the sensing signal-to-interference-plus-noise ratio (SINR). In addition, near-field beamforming was designed to maximize the beampattern gain under communication SINR constraints [8].

Despite the extensive research progress, the aforementioned works [6]–[8] consider fully-digital beamforming or fully-connected hybrid beamforming, which inevitably lead to prohibitive hardware cost and energy consumption, especially when large-scale antenna arrays are deployed. Moreover, the existing works [6]–[8] mainly focus on the sensing-centric optimization, while the communication-centric optimization has been not thoroughly investigated. Motivated by the above issues, we aim to analyze the performance boundary of near-field target localization and investigate the performance tradeoff between near-field localization and communication.

In this paper, we investigate partially-connected hybrid beamforming design for near-field millimeter-wave (mmWave) ISAC systems. To characterize the near-field target localization accuracy, we derive the squared position error bound (SPEB) for estimating the two-dimensional (2D) coordinates of target. The hybrid beamforming design is formulated as the sum-rate maximization under the SPEB constraint for target localization accuracy. This problem is first reformulated as a tractable form by exploiting the fractional programming (FP) method. Then, we propose a successive convex approximation (SCA)-based block coordinate descent (BCD) algorithm to tackle the nonconvex problem. Simulation results show that the proposed hybrid beamforming achieves sum-rate similar to the corresponding fully-digital beamforming and significantly outperforms the existing methods.

II. System Model

We consider a near-field mmWave ISAC system, where the base station (BS) simultaneously serves K single-antenna communication users (CUs) and locates one sensing target by exploiting the echo signal. Specifically, the BS is composed of an ISAC transmitter (Tx) equipped with N antennas and a sensing receiver (Rx) equipped with N antennas and is

capable of achieving perfect self-interference cancellation [6]. Without loss of generality, we assume that both Tx and Rx are equipped with uniform linear arrays (ULAs) with the antenna spacing of d, resulting in the array aperture of $D = (N-1)\,d$. Therefore, the Rayleigh distance is equal to $\frac{2D^2}{\lambda}$, where λ is the signal wavelength. It is assumed that both the CUs and sensing target are located in the near-field region of the BS. Let $\mathbf{p}_n^{\mathrm{BS}} = [x_n^{\mathrm{BS}}, y_n^{\mathrm{BS}}]^T, n = 1, \ldots, N$ denote the position of the n-th antenna of the Tx/Rx, $\mathbf{p}_k^{\mathrm{CU}} = [x_k, y_k]^T, k = 1, \ldots, K$ denote the position of the k-th CU, and $\mathbf{p}^{\mathrm{ST}} = [x, y]^T$ denote the position of the sensing target.

To reduce the hardware cost and energy consumption, partially-connected hybrid beamforming is considered at the Tx. Specifically, the Tx is equipped with N_{RF} radio frequency (RF) chains, each of which is connected to a subarray with $M = N/N_{\mathrm{RF}}$ antennas through phase shifters. With the partially-connected architecture, the analog beamformer of the Tx can be represented as

$$\mathbf{F}_{\mathrm{A}} = \mathrm{blkdiag}\left\{\mathbf{f}_1, \ldots, \mathbf{f}_{N_{\mathrm{RF}}}\right\}, \tag{1}$$

where $\mathbf{f}_i \in \mathbb{C}^{M\times 1}$ represents the analog beamforming vector corresponding to the i-th subarray with each element satisfying the constant modulus constraint, i.e., $\left|\left[\mathbf{f}_i\right]_j\right| = 1, i = 1, \ldots, N_{\mathrm{RF}}, j = 1, \ldots, M$.

A. Near-Field Channel Model

1) Communication Channel Model: We assume that the center of the Tx/Rx arrays is located at the origin of the coordinate system, i.e., $[0, 0]^T$. The position of the n-th antenna of the Tx/Rx can be denoted as $\mathbf{p}_n^{\mathrm{BS}} = [0, \delta_n d]^T$, where $\delta_n = \frac{2n-N-1}{2}, n = 1, \ldots, N$ [2]. The distance from the n-th antenna of the Tx/Rx to the k-th CU can be calculated as

$$||\mathbf{p}_k^{\mathrm{CU}} - \mathbf{p}_n^{\mathrm{BS}}|| = \sqrt{x_k^2 + y_k^2 - 2\delta_n d y_k + \delta_n^2 d^2}. \tag{2}$$

Thus, the near-field steering vector of the line-of-sight (LoS) path can be given by

$$\mathbf{a}\left(x_k, y_k\right) = \left[e^{-j\frac{2\pi}{\lambda}||\mathbf{p}_k^{\mathrm{CU}} - \mathbf{p}_1^{\mathrm{BS}}||}, \ldots, e^{-j\frac{2\pi}{\lambda}||\mathbf{p}_k^{\mathrm{CU}} - \mathbf{p}_N^{\mathrm{BS}}||}\right]^T. \tag{3}$$

Adopting the Saleh-Valenzuela model [2], the mmWave channel between the Tx and the k-th CU can be expressed as

$$\mathbf{h}_k = \alpha_k^{\mathrm{LoS}}\mathbf{a}\left(x_k, y_k\right) + \sum_{l=1}^{L_k}\alpha_{k,l}^{\mathrm{NLoS}}\mathbf{a}\left(x_{k,l}, y_{k,l}\right), \tag{4}$$

where α_k^{LoS} represents the complex gain of the LoS path, L_k represents the number of non-line-of-sight (NLoS) paths, $\alpha_{k,l}^{\mathrm{NLoS}}$ represents the complex gain of the l-th NLoS path, and $\mathbf{a}\left(x_{k,l}, y_{k,l}\right)$ represents the near-field steering vector corresponding to the l-th scatterer associated with the k-th CU.

2) Sensing Channel Model: The distance from the n-th antenna of the Tx/Rx to the sensing target can be calculated as

$$||\mathbf{p}^{\mathrm{ST}} - \mathbf{p}_n^{\mathrm{BS}}|| = \sqrt{x^2 + y^2 - 2\delta_n d y + \delta_n^2 d^2}. \tag{5}$$

Therefore, the near-field sensing channel can be expressed as

$$\mathbf{G} = \beta\mathbf{a}\left(x, y\right)\mathbf{a}^H\left(x, y\right), \tag{6}$$

where β represents the target reflection coefficient including both the distance-dependent path loss and the radar cross section (RCS) of the target, and $\mathbf{a}\left(x, y\right)$ represents the near-field steering vector, given by

$$\mathbf{a}\left(x, y\right) = \left[e^{-j\frac{2\pi}{\lambda}||\mathbf{p}^{\mathrm{ST}} - \mathbf{p}_1^{\mathrm{BS}}||}, \ldots, e^{-j\frac{2\pi}{\lambda}||\mathbf{p}^{\mathrm{ST}} - \mathbf{p}_N^{\mathrm{BS}}||}\right]^T. \tag{7}$$

B. Near-Field Signal Model

1) Communication Signal Model: For downlink multiuser communication, the signal transmitted by the Tx at the time instant t can be expressed as

$$\mathbf{x}(t) = \mathbf{F}_{\mathrm{A}}\mathbf{F}_{\mathrm{D}}\mathbf{s}(t) = \mathbf{F}_{\mathrm{A}}\sum_{k=1}^{K}\mathbf{f}_{\mathrm{D},k}s_k(t), \tag{8}$$

where $\mathbf{s}(t) = [s_1(t), \ldots, s_K(t)] \in \mathbb{C}^{K\times 1}$ represents the transmitted data symbol such that $\mathbb{E}\{\mathbf{s}(t)\mathbf{s}^H(t)\} = \mathbf{I}_K$, $\mathbf{F}_{\mathrm{D}} = [\mathbf{f}_{\mathrm{D},1}, \ldots, \mathbf{f}_{\mathrm{D},K}] \in \mathbb{C}^{N_{\mathrm{RF}}\times K}$ represents the digital beamformer, and $\mathbf{F}_{\mathrm{A}} \in \mathbb{C}^{N\times N_{\mathrm{RF}}}$ represents the analog beamformer.

The received signal of the k-th CU can be expressed as

$$y_{\mathrm{c},k}(t) = \mathbf{h}_k^H\mathbf{F}_{\mathrm{A}}\mathbf{f}_{\mathrm{D},k}s_k(t) + \sum_{j=1,j\neq k}^{K}\mathbf{h}_k^H\mathbf{F}_{\mathrm{A}}\mathbf{f}_{\mathrm{D},j}s_j(t) + z_{\mathrm{c},k}(t), \tag{9}$$

where $z_{\mathrm{c},k}(t)$ represents the Gaussian noise obeying $\mathcal{CN}(0, \sigma^2)$.

The SINR of the k-th CU can be represented as

$$\mathrm{SINR}_k = \frac{\left|\mathbf{h}_k^H\mathbf{F}_{\mathrm{A}}\mathbf{f}_{\mathrm{D},k}\right|^2}{\sum_{j=1,j\neq k}^{K}\left|\mathbf{h}_k^H\mathbf{F}_{\mathrm{A}}\mathbf{f}_{\mathrm{D},j}\right|^2 + \sigma^2}. \tag{10}$$

2) Sensing Signal Model: For target sensing, the echo signal received by the Rx at the t-th snapshot can be expressed as

$$\mathbf{y}_{\mathrm{s}}(t) = \beta\mathbf{a}\left(x, y\right)\mathbf{a}^H\left(x, y\right)\mathbf{x}(t) + \mathbf{z}_{\mathrm{s}}(t), \tag{11}$$

where $\mathbf{z}_{\mathrm{s}}(t) \in \mathbb{C}^{N\times 1}$ represents the Gaussian noise obeying $\mathcal{CN}(0, \sigma^2\mathbf{I}_N)$. The received echo signal over T snapshots can be represented as

$$\mathbf{Y}_{\mathrm{s}} = \beta\mathbf{a}\left(x, y\right)\mathbf{a}^H\left(x, y\right)\mathbf{X} + \mathbf{Z}_{\mathrm{s}}, \tag{12}$$

where $\mathbf{Y}_{\mathrm{s}} = [\mathbf{y}_{\mathrm{s}}(1), \ldots, \mathbf{y}_{\mathrm{s}}(T)]$, $\mathbf{X} = [\mathbf{x}(1), \ldots, \mathbf{x}(T)]$, and $\mathbf{Z}_{\mathrm{s}} = [\mathbf{z}_{\mathrm{s}}(1), \ldots, \mathbf{z}_{\mathrm{s}}(T)]$. Let $\mathbf{S} = [\mathbf{s}(1), \ldots, \mathbf{s}(T)]$ denote the transmitted symbol over T snapshots. Thus, the transmit covariance matrix can be represented as

$$\mathbf{R}_{\mathrm{X}} = \frac{1}{T}\mathbf{X}\mathbf{X}^H = \frac{1}{T}\mathbf{F}_{\mathrm{A}}\mathbf{F}_{\mathrm{D}}\mathbf{S}\mathbf{S}^H\mathbf{F}_{\mathrm{D}}^H\mathbf{F}_{\mathrm{A}}^H \approx \mathbf{F}_{\mathrm{A}}\mathbf{F}_{\mathrm{D}}\mathbf{F}_{\mathrm{D}}^H\mathbf{F}_{\mathrm{A}}^H. \tag{13}$$

Notice that this approximation in (13) can be regarded as an accurate equality when T is sufficiently large [9].

III. SPEB Analysis and Problem Formulation

A. SPEB Analysis

The target localization accuracy is typically measured by the SPEB [10], [11]. Different from using the CRB to evaluate the performance of joint distance and angle estimation in the existing work [6], we exploit the SPEB to intuitively characterize the near-field target localization accuracy in this

paper. To facilitate the SPEB analysis, the received echo signal in (12) can be vectorized as

$$\tilde{\mathbf{y}}_{\mathrm{s}} = \mathrm{vec}\left(\mathbf{Y}_{\mathrm{s}}\right) = \boldsymbol{\eta} + \tilde{\mathbf{z}}_{\mathrm{s}}, \tag{14}$$

where $\boldsymbol{\eta} = \beta \mathrm{vec}\left(\mathbf{a}\left(x,y\right)\mathbf{a}^H\left(x,y\right)\mathbf{X}\right) \in \mathbb{C}^{NT\times 1}$, and $\tilde{\mathbf{z}}_{\mathrm{s}} = \mathrm{vec}\left(\mathbf{Z}_{\mathrm{s}}\right)$ follows the Gaussian distribution $\mathcal{CN}(0,\sigma^2\mathbf{I}_{NT})$. Let $\boldsymbol{\xi} = [\mathbf{p}^{\mathrm{ST}}, \tilde{\boldsymbol{\beta}}]^T \in \mathbb{R}^{4\times 1}$ denote the vector of unknown parameters, where $\mathbf{p}^{\mathrm{ST}} = [x,y]^T$ is the target position parameter of interest, $\tilde{\boldsymbol{\beta}} = [\mathrm{Re}\left\{\beta\right\}, \mathrm{Im}\left\{\beta\right\}]^T$ is the nuisance parameter [10]. For notational convenience, let $\mathbf{A} = \mathbf{a}\left(x,y\right)\mathbf{a}^H\left(x,y\right)$.

Then, we derive the Fisher information matrix (FIM) for estimating the unknown parameters $\boldsymbol{\xi}$ from $\tilde{\mathbf{y}}_{\mathrm{s}}$. According to [9], the FIM for estimating $\boldsymbol{\xi}$ can be partitioned as

$$\mathbf{J}\left(\boldsymbol{\xi}\right) = \begin{bmatrix} \mathbf{J}_{xx} & \mathbf{J}_{xy} & \mathbf{J}_{x\tilde{\boldsymbol{\beta}}} \\ \mathbf{J}_{xy}^T & \mathbf{J}_{yy} & \mathbf{J}_{y\tilde{\boldsymbol{\beta}}} \\ \mathbf{J}_{x\tilde{\boldsymbol{\beta}}}^T & \mathbf{J}_{y\tilde{\boldsymbol{\beta}}}^T & \mathbf{J}_{\tilde{\boldsymbol{\beta}}\tilde{\boldsymbol{\beta}}} \end{bmatrix} \in \mathbb{R}^{4\times 4}, \tag{15}$$

where

$$\mathbf{J}_{xx} = \frac{2T|\beta|^2}{\sigma^2}\mathrm{tr}\left(\dot{\mathbf{A}}_x\mathbf{F}_{\mathrm{A}}\mathbf{F}_{\mathrm{D}}\mathbf{F}_{\mathrm{D}}^H\mathbf{F}_{\mathrm{A}}^H\dot{\mathbf{A}}_x^H\right), \tag{16a}$$

$$\mathbf{J}_{xy} = \frac{2T|\beta|^2}{\sigma^2}\mathrm{tr}\left(\dot{\mathbf{A}}_y\mathbf{F}_{\mathrm{A}}\mathbf{F}_{\mathrm{D}}\mathbf{F}_{\mathrm{D}}^H\mathbf{F}_{\mathrm{A}}^H\dot{\mathbf{A}}_x^H\right), \tag{16b}$$

$$\mathbf{J}_{yy} = \frac{2T|\beta|^2}{\sigma^2}\mathrm{tr}\left(\dot{\mathbf{A}}_y\mathbf{F}_{\mathrm{A}}\mathbf{F}_{\mathrm{D}}\mathbf{F}_{\mathrm{D}}^H\mathbf{F}_{\mathrm{A}}^H\dot{\mathbf{A}}_y^H\right), \tag{16c}$$

$$\mathbf{J}_{x\tilde{\boldsymbol{\beta}}} = \frac{2T}{\sigma^2}\mathrm{Re}\left\{\beta^*\mathrm{tr}(\mathbf{A}\mathbf{F}_{\mathrm{A}}\mathbf{F}_{\mathrm{D}}\mathbf{F}_{\mathrm{D}}^H\mathbf{F}_{\mathrm{A}}^H\dot{\mathbf{A}}_x^H)[1,j]\right\}, \tag{16d}$$

$$\mathbf{J}_{y\tilde{\boldsymbol{\beta}}} = \frac{2T}{\sigma^2}\mathrm{Re}\left\{\beta^*\mathrm{tr}(\mathbf{A}\mathbf{F}_{\mathrm{A}}\mathbf{F}_{\mathrm{D}}\mathbf{F}_{\mathrm{D}}^H\mathbf{F}_{\mathrm{A}}^H\dot{\mathbf{A}}_y^H)[1,j]\right\}, \tag{16e}$$

$$\mathbf{J}_{\tilde{\boldsymbol{\beta}}\tilde{\boldsymbol{\beta}}} = \frac{2T}{\sigma^2}\mathrm{tr}\left(\mathbf{A}\mathbf{F}_{\mathrm{A}}\mathbf{F}_{\mathrm{D}}\mathbf{F}_{\mathrm{D}}^H\mathbf{F}_{\mathrm{A}}^H\mathbf{A}^H\right)\mathbf{I}_2, \tag{16f}$$

and $\dot{\mathbf{A}}_x = \frac{\partial \mathbf{A}_x}{\partial x}$ and $\dot{\mathbf{A}}_y = \frac{\partial \mathbf{A}_y}{\partial y}$ represent the partial derivatives of $\mathbf{A}$ with respect to x and y, respectively.

For notational simplicity, we define

$$\mathbf{J}_{11} = \begin{bmatrix} \mathbf{J}_{xx} & \mathbf{J}_{xy} \\ \mathbf{J}_{xy}^T & \mathbf{J}_{yy} \end{bmatrix}, \quad \mathbf{J}_{12} = \begin{bmatrix} \mathbf{J}_{x\tilde{\boldsymbol{\beta}}} \\ \mathbf{J}_{y\tilde{\boldsymbol{\beta}}} \end{bmatrix}, \quad \mathbf{J}_{22} = \mathbf{J}_{\tilde{\boldsymbol{\beta}}\tilde{\boldsymbol{\beta}}}. \tag{17}$$

By isolating the impact of the nuisance parameter $\tilde{\boldsymbol{\beta}}$, the equivalent FIM [10] of the target position $[x,y]^T$ can be expressed as

$$\mathbf{J}_{\mathrm{e}}(x,y) = \mathbf{J}_{11} - \mathbf{J}_{12}\mathbf{J}_{22}^{-1}\mathbf{J}_{12}^T. \tag{18}$$

Therefore, the SPEB of near-field target localization can be represented as

$$\mathrm{SPEB} = \mathrm{tr}\left(\left(\mathbf{J}_{\mathrm{e}}(x,y)\right)^{-1}\right). \tag{19}$$

From (15), (16), (17), (18), and (19), we observe that the SPEB can be expressed as a function of the hybrid beamforming matrix $\mathbf{F}_{\mathrm{A}}\mathbf{F}_{\mathrm{D}}$. Therefore, we can enhance the target localization accuracy by optimizing the hybrid beamforming design.

B. Problem Formulation

We aim to jointly design the digital beamformer and analog beamformer to maximize the sum-rate of CUs, while ensuring the target localization accuracy requirement, transmit power constraint, and constant modulus constraints. The hybrid beamforming design can be formulated as

$$\max_{\mathbf{F}_{\mathrm{A}},\mathbf{F}_{\mathrm{D}}} \sum_{k=1}^{K}\log\left(1+\mathrm{SINR}_k\right) \tag{20a}$$

$$\text{s.t.} \quad \mathrm{SPEB} \le \Gamma_s, \tag{20b}$$

$$\left\|\mathbf{F}_{\mathrm{A}}\mathbf{F}_{\mathrm{D}}\right\|_F^2 \le P, \tag{20c}$$

$$\mathbf{F}_{\mathrm{A}} \in \mathcal{A}, \tag{20d}$$

where Γ_s represents the SPEB threshold of target localization, P represents the transmit power budget, and $\mathcal{A}$ represents the feasible set of partially-connected analog beamformer in which constant modulus constraints are imposed on the nonzero elements of $\mathbf{F}_{\mathrm{A}}$. Notice that problem (20) is intractable due to the nonconvex objective function, highly coupled optimization variables, and nonconvex constant modulus constraints.

IV. Hybrid Beamforming Design

A. Problem Reformulation

The objective function in (20a) is first reformulated as a tractable form by exploiting the FP technique. Based on the Lagrangian dual transform [12], we introduce the auxiliary variable $\boldsymbol{\gamma} = [\gamma_1,\ldots,\gamma_K]^T \in \mathbb{R}_+^{K\times 1}$ and equivalently recast the objective function in (20a) as

$$\sum_{k=1}^{K}\log\left(1+\gamma_k\right) - \sum_{k=1}^{K}\gamma_k + \sum_{k=1}^{K}\frac{\left(1+\gamma_k\right)\left|\mathbf{h}_k^H\mathbf{F}_{\mathrm{A}}\mathbf{f}_{\mathrm{D},k}\right|^2}{\sum_{j=1}^{K}\left|\mathbf{h}_k^H\mathbf{F}_{\mathrm{A}}\mathbf{f}_{\mathrm{D},j}\right|^2+\sigma^2}. \tag{21}$$

Then, the quadratic transform [12] is applied to tackle the sum-of-ratio term in (21). By introducing the auxiliary variable $\boldsymbol{\mu} = [\mu_1,\ldots,\mu_K]^T \in \mathbb{C}^{K\times 1}$, the objective function in (21) can be reformulated as

$$f\left(\mathbf{F}_{\mathrm{A}},\mathbf{F}_{\mathrm{D}},\boldsymbol{\gamma},\boldsymbol{\mu}\right) = \sum_{k=1}^{K}\log\left(1+\gamma_k\right) - \sum_{k=1}^{K}\gamma_k - \sum_{k=1}^{K}\left|\mu_k\right|^2\sigma^2$$
$$-\sum_{k=1}^{K}\sum_{j=1}^{K}\left|\mu_k\right|^2\left|\mathbf{h}_k^H\mathbf{F}_{\mathrm{A}}\mathbf{f}_{\mathrm{D},j}\right|^2 + \sum_{k=1}^{K}2\sqrt{\left(1+\gamma_k\right)}\mathrm{Re}\left\{\mu_k^*\mathbf{h}_k^H\mathbf{F}_{\mathrm{A}}\mathbf{f}_{\mathrm{D},k}\right\}. \tag{22}$$

Therefore, problem (20) can be reformulated as

$$\max_{\mathbf{F}_{\mathrm{A}},\mathbf{F}_{\mathrm{D}},\boldsymbol{\gamma},\boldsymbol{\mu}} \; f\left(\mathbf{F}_{\mathrm{A}},\mathbf{F}_{\mathrm{D}},\boldsymbol{\gamma},\boldsymbol{\mu}\right) \tag{23a}$$

$$\text{s.t.} \quad (20\text{b}),(20\text{c}),(20\text{d}). \tag{23b}$$

To address problem (23), the BCD framework is employed to optimize the analog beamformer $\mathbf{F}_{\mathrm{A}}$, digital beamformer $\mathbf{F}_{\mathrm{D}}$, and auxiliary variables $\boldsymbol{\gamma}$ and $\boldsymbol{\mu}$ in an alternating manner.

With the other variables fixed, the subproblem with respect to γ_k and the subproblem with respect to μ_k are unconstrained convex problems. Based on the first-order optimality condition,

the optimal closed-form solutions of γ_k and μ_k can be respectively given by

$$\gamma_k^\star = \frac{\left|\mathbf{h}_k^H \mathbf{F}_\mathrm{A} \mathbf{f}_{\mathrm{D},k}\right|^2}{\sum_{j=1,j\neq k}^K \left|\mathbf{h}_k^H \mathbf{F}_\mathrm{A} \mathbf{f}_{\mathrm{D},j}\right|^2 + \sigma^2}, \forall k, \tag{24a}$$

$$\mu_k^\star = \frac{\sqrt{(1+\gamma_k)}\mathbf{h}_k^H \mathbf{F}_\mathrm{A} \mathbf{f}_{\mathrm{D},k}}{\sum_{j=1}^K \left|\mathbf{h}_k^H \mathbf{F}_\mathrm{A} \mathbf{f}_{\mathrm{D},j}\right|^2 + \sigma^2}, \forall k. \tag{24b}$$

B. Analog Beamformer Design

In this subsection, we optimize the analog beamformer $\mathbf{F}_\mathrm{A}$ with the digital beamformer $\mathbf{F}_\mathrm{D}$ and the auxiliary variables $\boldsymbol{\gamma}$ and $\boldsymbol{\mu}$ fixed. Utilizing the block diagonal structure, the analog beamformer can be rewritten as

$$\mathbf{F}_\mathrm{A} = \tilde{\mathbf{F}}_\mathrm{A} \boldsymbol{\Phi} = \mathrm{diag}\left(\mathbf{f}_\mathrm{A}\right) \boldsymbol{\Phi}, \tag{25}$$

where $\tilde{\mathbf{F}}_\mathrm{A} = \mathrm{blkdiag}\left\{\mathrm{diag}\left(\mathbf{f}_1\right), \ldots, \mathrm{diag}\left(\mathbf{f}_{N_\mathrm{RF}}\right)\right\} \in \mathbb{C}^{N\times N}$ and $\mathbf{f}_\mathrm{A} = [\mathbf{f}_1^T, \cdots, \mathbf{f}_{N_\mathrm{RF}}^T]^T \in \mathbb{C}^{N\times 1}$ represent a diagonal matrix and a column vector composed of the nonzero elements of $\mathbf{F}_\mathrm{A}$, respectively, $\boldsymbol{\Phi} = \mathrm{blkdiag}\left\{\mathbf{1}_M, \cdots, \mathbf{1}_M\right\} \in \mathbb{C}^{N\times N_\mathrm{RF}}$ represents a block diagonal matrix in which $\mathbf{1}_M \in \mathbb{C}^{M\times 1}$ is a column vector with each element being 1. Therefore, the transmit covariance matrix in (13) can be rewritten as

$$\begin{aligned}\mathbf{R}_\mathrm{X} &= \sum_{k=1}^K \mathrm{diag}\left(\mathbf{f}_\mathrm{A}\right) \boldsymbol{\Phi} \mathbf{f}_{\mathrm{D},k} \mathbf{f}_{\mathrm{D},k}^H \boldsymbol{\Phi}^H \mathrm{diag}\left(\mathbf{f}_\mathrm{A}\right)^H \\ &= \sum_{k=1}^K \mathrm{diag}\left(\boldsymbol{\Phi}\mathbf{f}_{\mathrm{D},k}\right) \mathbf{f}_\mathrm{A} \mathbf{f}_\mathrm{A}^H \mathrm{diag}\left(\boldsymbol{\Phi}\mathbf{f}_{\mathrm{D},k}\right)^H. \end{aligned} \tag{26}$$

For notational convenience, we define

$$\mathbf{J}_{11}\left(\mathbf{f}_\mathrm{A}\right) = \frac{2T|\beta|^2}{\sigma^2} \mathrm{Re}\left\{\begin{bmatrix} \mathrm{tr}(\dot{\mathbf{A}}_x \mathbf{R}_\mathrm{X} \dot{\mathbf{A}}_x^H) & \mathrm{tr}(\dot{\mathbf{A}}_y \mathbf{R}_\mathrm{X} \dot{\mathbf{A}}_x^H) \\ \mathrm{tr}(\dot{\mathbf{A}}_x \mathbf{R}_\mathrm{X} \dot{\mathbf{A}}_y^H) & \mathrm{tr}(\dot{\mathbf{A}}_y \mathbf{R}_\mathrm{X} \dot{\mathbf{A}}_y^H) \end{bmatrix}\right\}, \tag{27a}$$

$$\mathbf{J}_{12}\left(\mathbf{f}_\mathrm{A}\right) = \frac{2T}{\sigma^2} \mathrm{Re}\left\{\begin{bmatrix} \beta^* \mathrm{tr}(\mathbf{A} \mathbf{R}_\mathrm{X} \dot{\mathbf{A}}_x^H) \\ \beta^* \mathrm{tr}(\mathbf{A} \mathbf{R}_\mathrm{X} \dot{\mathbf{A}}_y^H) \end{bmatrix} [1, j]\right\}, \tag{27b}$$

$$\mathbf{J}_{22}\left(\mathbf{f}_\mathrm{A}\right) = \frac{2T}{\sigma^2} \mathrm{tr}(\mathbf{A} \mathbf{R}_\mathrm{X} \mathbf{A}^H) \mathbf{I}_2, \tag{27c}$$

$$\mathbf{B} = \sum_{j=1}^K \mathrm{diag}\left(\boldsymbol{\Phi}\mathbf{f}_{\mathrm{D},j}\right)^H \left(\sum_{k=1}^K \left|\mu_k\right|^2 \mathbf{h}_k \mathbf{h}_k^H\right) \mathrm{diag}\left(\boldsymbol{\Phi}\mathbf{f}_{\mathrm{D},j}\right), \tag{27d}$$

$$\mathbf{c} = \sum_{k=1}^K \sqrt{(1+\gamma_k)} \mu_k \mathrm{diag}\left(\boldsymbol{\Phi}\mathbf{f}_{\mathrm{D},j}\right)^H \mathbf{h}_k. \tag{27e}$$

To tackle the SPEB constraint in (20b), we introduce the auxiliary positive semidefinite matrix $\mathbf{U} \in \mathbb{C}^{2\times 2}$. Thus, the subproblem with respect to $\mathbf{f}_\mathrm{A}$ can be reformulated as

$$\min_{\mathbf{f}_\mathrm{A}, \mathbf{U}} \ \mathbf{f}_\mathrm{A}^H \mathbf{B} \mathbf{f}_\mathrm{A} - 2\mathrm{Re}\left\{\mathbf{f}_\mathrm{A}^H \mathbf{c}\right\} \tag{28a}$$

$$\text{s.t. } \mathrm{tr}\left(\mathbf{U}^{-1}\right) \leq \Gamma_s, \tag{28b}$$

$$\mathbf{U} \succeq \mathbf{0}, \tag{28c}$$

$$\begin{bmatrix} \mathbf{J}_{11}\left(\mathbf{f}_\mathrm{A}\right) - \mathbf{U} & \mathbf{J}_{12}\left(\mathbf{f}_\mathrm{A}\right) \\ \mathbf{J}_{12}^T\left(\mathbf{f}_\mathrm{A}\right) & \mathbf{J}_{22}\left(\mathbf{f}_\mathrm{A}\right) \end{bmatrix} \succeq \mathbf{0}, \tag{28d}$$

$$\left|\left[\mathbf{f}_\mathrm{A}\right]_i\right| = 1, \forall i. \tag{28e}$$

Note that problem (28) is a nonconvex quadratically constrained quadratic programming (QCQP) problem due to the quadratic objective function in (28a), nonconvex quadratic constraint in (28d), and nonconvex constant modulus constraints in (28e). To address the nonconvex problem, we introduce the auxiliary variable $\mathbf{R}_\mathrm{A} = \mathbf{f}_\mathrm{A} \mathbf{f}_\mathrm{A}^H$ such that $\mathbf{R}_\mathrm{A} \succeq \mathbf{0}$ and $\mathrm{rank}\left(\mathbf{R}_\mathrm{A}\right) = 1$. By omitting nonconvex rank-one constraint, problem (28) can be relaxed as

$$\min_{\mathbf{R}_\mathrm{A}, \mathbf{f}_\mathrm{A}, \mathbf{U}} \ \mathrm{tr}\left(\mathbf{B}\mathbf{R}_\mathrm{A}\right) - 2\mathrm{Re}\left\{\mathbf{f}_\mathrm{A}^H \mathbf{c}\right\} \tag{29a}$$

$$\text{s.t. } \begin{bmatrix} \mathbf{J}_{11}\left(\mathbf{R}_\mathrm{A}\right) - \mathbf{U} & \mathbf{J}_{12}\left(\mathbf{R}_\mathrm{A}\right) \\ \mathbf{J}_{12}^T\left(\mathbf{R}_\mathrm{A}\right) & \mathbf{J}_{22}\left(\mathbf{R}_\mathrm{A}\right) \end{bmatrix} \succeq \mathbf{0}, \tag{29b}$$

$$\left|\left[\mathbf{R}_\mathrm{A}\right]_{i,i}\right| = 1, \forall i, \tag{29c}$$

$$\mathbf{R}_\mathrm{A} = \mathbf{f}_\mathrm{A} \mathbf{f}_\mathrm{A}^H, \tag{29d}$$

$$\mathbf{R}_\mathrm{A} \succeq \mathbf{0}, \tag{29e}$$

$$(28b), (28c). \tag{29f}$$

Nevertheless, problem (29) is still nonconvex owing to the nonconvex equality constraint in (29d). The equality constraint $\mathbf{R}_\mathrm{A} = \mathbf{f}_\mathrm{A} \mathbf{f}_\mathrm{A}^H$ can be equivalently transformed into the two inequality constraints as follows:

$$\begin{bmatrix} \mathbf{R}_\mathrm{A} & \mathbf{f}_\mathrm{A} \\ \mathbf{f}_\mathrm{A}^H & 1 \end{bmatrix} \succeq \mathbf{0}, \tag{30a}$$

$$\mathrm{tr}\left(\mathbf{R}_\mathrm{A}\right) - \mathbf{f}_\mathrm{A}^H \mathbf{f}_\mathrm{A} \leq 0. \tag{30b}$$

However, constraint (30b) is nonconvex. Utilizing the SCA technique, the convex approximation of constraint (30b) can be represented as

$$\mathrm{tr}\left(\mathbf{R}_\mathrm{A}\right) - 2\mathrm{Re}\left\{\left(\mathbf{f}_\mathrm{A}^{(n)}\right)^H \mathbf{f}_\mathrm{A}\right\} + \left(\mathbf{f}_\mathrm{A}^{(n)}\right)^H \mathbf{f}_\mathrm{A}^{(n)} \leq 0. \tag{31}$$

where $\mathbf{f}_\mathrm{A}^{(n)}$ is the solution obtained at the n-th iteration. Therefore, the convex approximation of problem (29) can be reformulated as

$$\min_{\mathbf{R}_\mathrm{A}, \mathbf{f}_\mathrm{A}, \mathbf{U}} \ \mathrm{tr}\left(\mathbf{B}\mathbf{R}_\mathrm{A}\right) - 2\mathrm{Re}\left\{\mathbf{f}_\mathrm{A}^H \mathbf{c}\right\} \tag{32a}$$

$$\text{s.t. } (28b), (28c), (29b), (29c), (29e), (30a), (31). \tag{32b}$$

We observe that problem (32) is a convex problem, which can be efficiently solved by CVX toolbox.

C. Digital Beamformer Design

With the analog beamformer $\mathbf{F}_\mathrm{A}$ and the auxiliary variables $\boldsymbol{\gamma}$ and $\boldsymbol{\mu}$ fixed, we optimize the digital beamformer $\mathbf{F}_\mathrm{D}$ in this subsection. The subproblem with respect to $\mathbf{F}_\mathrm{D}$ can be reformulated as

$$\min_{\mathbf{F}_\mathrm{D}, \mathbf{U}} \ \sum_{k=1}^K \mathbf{f}_{\mathrm{D},k}^H \mathbf{D} \mathbf{f}_{\mathrm{D},k} - \sum_{k=1}^K 2\mathrm{Re}\left\{\mathbf{f}_{\mathrm{D},k}^H \mathbf{e}_k\right\} \tag{33a}$$

$$\text{s.t. } \mathrm{tr}\left(\mathbf{U}^{-1}\right) \leq \Gamma_s, \tag{33b}$$

$$\mathbf{U} \succeq \mathbf{0}, \tag{33c}$$

$$\begin{bmatrix} \mathbf{J}_{11}\left(\mathbf{F}_\mathrm{D}\right) - \mathbf{U} & \mathbf{J}_{12}\left(\mathbf{F}_\mathrm{D}\right) \\ \mathbf{J}_{12}^T\left(\mathbf{F}_\mathrm{D}\right) & \mathbf{J}_{22}\left(\mathbf{F}_\mathrm{D}\right) \end{bmatrix} \succeq \mathbf{0}, \tag{33d}$$

$$\mathrm{tr}\left(\mathbf{F}_\mathrm{D} \mathbf{F}_\mathrm{D}^H\right) \leq P/M, \tag{33e}$$

where we define

$$\mathbf{D} = \sum_{k=1}^{K} |\mu_k|^2 \mathbf{F}_{\mathrm{A}}^H \mathbf{h}_k \mathbf{h}_k^H \mathbf{F}_{\mathrm{A}}, \tag{34a}$$

$$\mathbf{e}_k = \sqrt{(1+\gamma_k)}\mu_k \mathbf{F}_{\mathrm{A}}^H \mathbf{h}_k. \tag{34b}$$

Problem (33) is also a nonconvex QCQP problem due to the quadratic objective function in (33a) and the nonconvex quadratic constraint in (33d). To tackle this problem, we introduce the auxiliary variables $\mathbf{R}_{\mathrm{D},k} = \mathbf{f}_{\mathrm{D},k}\mathbf{f}_{\mathrm{D},k}^H, \forall k$ such that $\mathbf{R}_{\mathrm{D},k} \succeq \mathbf{0}$ and $\mathrm{rank}\left(\mathbf{R}_{\mathrm{D},k}\right) = 1, \forall k$. By dropping nonconvex rank-one constraints, problem (33) can be relaxed as

$$\min_{\mathbf{R}_{\mathrm{D},k}, \mathbf{f}_{\mathrm{D},k}, \mathbf{U}} \mathrm{tr}\left(\mathbf{D}\sum_{k=1}^{K}\mathbf{R}_{\mathrm{D},k}\right) - \sum_{k=1}^{K} 2\mathrm{Re}\left\{\mathbf{f}_{\mathrm{D},k}^H \mathbf{e}_k\right\} \tag{35a}$$

$$\text{s.t.} \begin{bmatrix} \mathbf{J}_{11}\left(\mathbf{R}_{\mathrm{D},k}\right) - \mathbf{U} & \mathbf{J}_{12}\left(\mathbf{R}_{\mathrm{D},k}\right) \\ \mathbf{J}_{12}^T\left(\mathbf{R}_{\mathrm{D},k}\right) & \mathbf{J}_{22}\left(\mathbf{R}_{\mathrm{D},k}\right) \end{bmatrix} \succeq \mathbf{0}, \tag{35b}$$

$$\mathrm{tr}\left(\sum_{k=1}^{K}\mathbf{R}_{\mathrm{D},k}\right) \leq P/M, \tag{35c}$$

$$\mathbf{R}_{\mathrm{D},k} = \mathbf{f}_{\mathrm{D},k}\mathbf{f}_{\mathrm{D},k}^H, \forall k, \tag{35d}$$

$$\mathbf{R}_{\mathrm{D},k} \succeq \mathbf{0}, \forall k, \tag{35e}$$

$$(33\mathrm{b}), (33\mathrm{c}). \tag{35f}$$

Notice that problem (35) is still nonconvex since the equality constraint in (35d) is nonconvex. Similarly, the equality constraint $\mathbf{R}_{\mathrm{D},k} = \mathbf{f}_{\mathrm{D},k}\mathbf{f}_{\mathrm{D},k}^H, \forall k$ can be equivalently converted into the following two inequality constraints:

$$\begin{bmatrix} \mathbf{R}_{\mathrm{D},k} & \mathbf{f}_{\mathrm{D},k} \\ \mathbf{f}_{\mathrm{D},k}^H & 1 \end{bmatrix} \succeq \mathbf{0}, \forall k, \tag{36a}$$

$$\mathrm{tr}\left(\mathbf{R}_{\mathrm{D},k}\right) - \mathbf{f}_{\mathrm{D},k}^H \mathbf{f}_{\mathrm{D},k} \leq 0, \forall k. \tag{36b}$$

By applying the SCA method, the nonconvex inequality constraint in (36b) can be approximated as

$$\mathrm{tr}\left(\mathbf{R}_{\mathrm{D},k}\right) - 2\mathrm{Re}\left\{\left(\mathbf{f}_{\mathrm{D},k}^{(n)}\right)^H \mathbf{f}_{\mathrm{D},k}\right\} + \left(\mathbf{f}_{\mathrm{D},k}^{(n)}\right)^H \mathbf{f}_{\mathrm{D},k}^{(n)} \leq 0, \forall k, \tag{37}$$

where $\mathbf{f}_{\mathrm{D},k}^{(n)}$ is the solution obtained at the n-th iteration. Therefore, the convex approximation of problem (35) can be reformulated as

$$\min_{\mathbf{R}_{\mathrm{D},k}, \mathbf{f}_{\mathrm{D},k}, \mathbf{U}} \mathrm{tr}\left(\mathbf{D}\sum_{k=1}^{K}\mathbf{R}_{\mathrm{D},k}\right) - \sum_{k=1}^{K} 2\mathrm{Re}\left\{\mathbf{f}_{\mathrm{D},k}^H \mathbf{e}_k\right\} \tag{38a}$$

$$\text{s.t. } (33\mathrm{b}), (33\mathrm{c}), (35\mathrm{b}), (35\mathrm{c}), (35\mathrm{e}), (36\mathrm{a}), (37). \tag{38b}$$

It is observed that problem (38) is a convex problem, which can be solved by CVX.

The proposed SCA-BCD algorithm for solving the sensing SPEB-constrained communication sum-rate maximization problem (20) is summarized in **Algorithm 1**. The initial value of the nonzero elements of the analog beamformer is set to 1. The digital beamformer is first randomly initialized, and then is normalized to satisfy the transmit power constraint.

Algorithm 1 Proposed SCA-BCD algorithm

1: **Input:** Analog beamformer $\mathbf{F}_{\mathrm{A}}^{(0)}$, digital beamformer $\mathbf{F}_{\mathrm{D}}^{(0)}$, iteration index $n = 1$.
2: **repeat**
3: Update $\boldsymbol{\gamma}^{(n)}$ by equation (24a);
4: Update $\boldsymbol{\mu}^{(n)}$ by equation (24b);
5: Update $\mathbf{F}_{\mathrm{A}}^{(n)}$ by solving problem (32);
6: Update $\mathbf{F}_{\mathrm{D}}^{(n)}$ by solving problem (38);
7: $n = n + 1$;
8: **until** The objective value of problem (20) is converged.
9: **Output:** $\mathbf{F}_{\mathrm{A}}$, $\mathbf{F}_{\mathrm{D}}$.

TABLE I
SIMULATION PARAMETERS

Notation	Definition	Value
N	Number of antennas at the Tx/Rx	32
N_{RF}	Number of RF chains at the Tx	4
K	Number of CUs	2
f_c	Carrier frequency	28 GHz
λ	Signal wavelength	1.07 cm
D	Array aperture	0.5 m
$\frac{2D^2}{\lambda}$	Rayleigh distance	46.7 m
P	Transmit power of the BS	30 dBm
σ^2	Noise power	-90 dBm
Γ_s	Sensing SPEB threshold	0.04 m^2
T	Number of snapshots	100

V. SIMULATION RESULTS

This section provides numerical simulations to verify the effectiveness of the proposed algorithm. Unless otherwise specified, the simulation parameters are set in Table I. Specifically, the CUs are randomly distributed on a semi-circle with the distance of 20m away from the BS and the angle ranging from $-\pi/2$ to $\pi/2$, and the target is located at (10m, 0). The large-scale fading is considered for multiuser communication and target sensing. To verify the effectiveness of our proposed SCA-BCD-based hybrid beamforming (labelled as **SCA-BCD-based HBF**), the baseline schemes are set as follows:

1) **SCA-BCD-based FDBF:** The fully-digital beamformer can also be designed by applying the proposed SCA-BCD algorithm.

2) **Matrix Approximation-based HBF:** As shown in [13], the digital beamformer and analog beamformer are alternately updated to minimize the Euclidean distance between the hybrid beamforming matrix and the fully-digital beamforming matrix obtained by **SCA-BCD-based FDBF**.

Fig. 1 shows the convergence behaviour of the proposed SCA-BCD algorithm. As the number of iterations increases, the sum-rate of the proposed SCA-BCD algorithm monotonically increases and converges within several iterations. Moreover, as the number of RF chains increases, the convergence speed can be improved due to the increased degrees of freedom in beamforming design.

Fig. 2 illustrates the sum-rate of the proposed algorithm under various transmit powers. We observe that the proposed

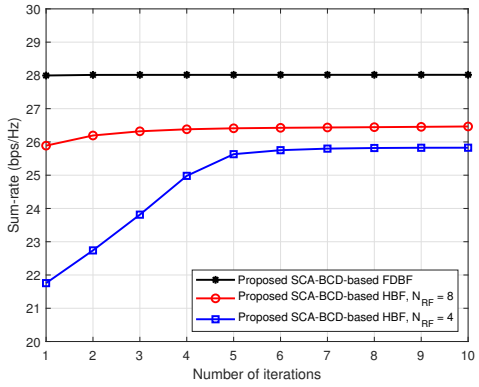

Fig. 1. Convergence of the proposed SCA-BCD algorithm.

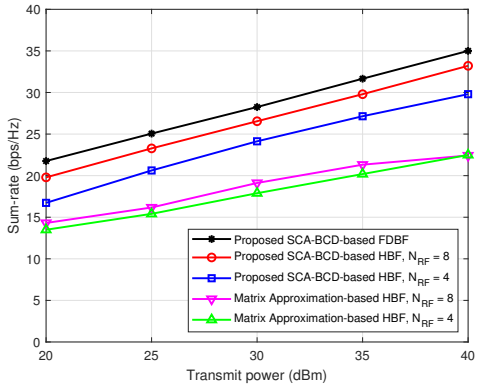

Fig. 2. Sum-rate versus transmit power.

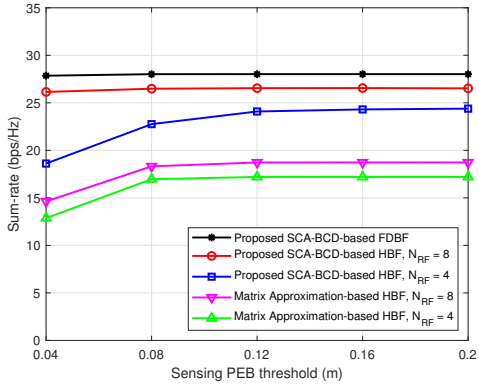

Fig. 3. Performance tradeoff between sum-rate and localization accuracy.

SCA-BCD-based hybrid beamforming can achieve performance close to the corresponding fully-digital counterpart when the number of RF chains is sufficiently large. In addition, the proposed SCA-BCD-based hybrid beamforming significantly outperforms the existing matrix approximation-based approach [13]. This is due to the fact that the matrix approximation-based hybrid beamforming is tailored for single-user communication-only systems [13] and inevitably causes interuser interference in multiuser ISAC systems, thereby leading to significant performance deterioration.

Fig. 3 depicts the tradeoff between communication sum-rate and target localization accuracy, where the sensing position error bound (PEB) threshold is the square root of sensing SPEB threshold, i.e. $\sqrt{\Gamma_s}$. As can be seen, the sum-rate achieved by the proposed SCA-BCD algorithm is improved as the sensing PEB threshold increases. In other words, the reduction of localization accuracy demand allows more power resource to be allocated to multiuser communication, thereby resulting in the improvement of communication sum-rate. Furthermore, as the number of RF chains increases, the performance gap between hybrid beamforming and fully-digital beamforming decreases, which reflects the tradeoff between system performance and hardware complexity.

VI. Concultion

This paper investigated hybrid beamforming design for near-field mmWave ISAC systems. The SPEB was first analyzed to characterize the near-field target localization accuracy. Then, the hybrid beamforming design was formulated as the sensing SPEB-constrained communication sum-rate maximization problem. To address the nonconvex problem, we proposed an SCA-BCD algorithm to obtain the locally optimal solution. Simulation results showed that the proposed SCA-BCD-based hybrid beamforming can achieve sum-rate similar to the corresponding fully-digital beamforming and significantly outperform the existing schemes.

References

[1] F. Liu et al., "Integrated sensing and communications: Toward dual functional wireless networks for 6G and beyond," *IEEE J. Sel. Areas Commun.*, vol. 40, no. 6, pp. 1728–1767, Jun. 2022.

[2] C. You et al., "Next generation advanced transceiver technologies for 6G and beyond," *IEEE J. Sel. Areas Commun.*, vol. 43, no. 3, pp. 582-627, Mar. 2025.

[3] M. Cui, Z. Wu, Y. Lu, X. Wei, and L. Dai, "Near-field MIMO communications for 6G: Fundamentals, challenges, potentials, and future directions," *IEEE Commun. Mag.*, vol. 61, no. 1, pp. 40–46, Jan. 2023.

[4] H. Zhang, N. Shlezinger, F. Guidi, D. Dardari, M. F. Imani, and Y. C. Eldar, "Beam focusing for near-field multiuser MIMO communications," *IEEE Trans. Wireless Commun.*, vol. 21, no. 9, pp. 7476–7490, Sep. 2022.

[5] J. Cong et al., "Near-field integrated sensing and communication: Opportunities and challenges," *IEEE Wireless Commun.*, vol. 31, no. 6, pp. 162–169, Dec. 2024.

[6] Z. Wang, X. Mu, and Y. Liu, "Near-field integrated sensing and communications," *IEEE Commun. Lett.*, vol. 27, no. 8, pp. 2048–2052, Aug. 2023.

[7] K. Qu, S. Guo, N. Saeed, and J. Ye, "Near-field integrated sensing and communication: Performance analysis and beamforming design," *IEEE Open J. Commun. Soc.*, vol. 5, pp. 6353–6366, 2024.

[8] P. Sun and B. Wang, "Near-field beam focusing for integrated sensing and communication systems," *IEEE Internet Things J.*, vol. 12, no. 12, pp. 18643-18650, Jun. 2025.

[9] I. Bekkerman and J. Tabrikian, "Target detection and localization using MIMO radars and sonars," *IEEE Trans. Signal Process.*, vol. 54, no. 10, pp. 3873–3883, Oct. 2006.

[10] Y. Shen and M. Z. Win, "Fundamental limits of wideband localization—Part I: A general framework," *IEEE Trans. Inf. Theory*, vol. 56, no. 10, pp. 4956–4980, Oct. 2010.

[11] N. González-Prelcic et al., "The integrated sensing and communication revolution for 6G: Vision, techniques, and applications," *Proc. IEEE*, vol. 112, no. 7, pp. 676-723, Jul. 2024.

[12] K. Shen and W. Yu, "Fractional programming for communication systems—Part I: Power control and beamforming," *IEEE Trans. Signal Process.*, vol. 66, no. 10, pp. 2616–2630, May 2018.

[13] X. Yu, J.-C. Shen, J. Zhang, and K. B. Letaief, "Alternating minimization algorithms for hybrid precoding in millimeter wave MIMO systems," *IEEE J. Sel. Topics Signal Process.*, vol. 10, no. 3, pp. 485–500, May 2016.